fractal and fractional

MDPI

Article

Dynamic Behavior and Optical Soliton for the M-Truncated Fractional Paraxial Wave Equation Arising in a Liquid Crystal Model

Jie Luo [1] and Zhao Li [2,*]

[1] School of Electronic Information and Electrical Engineering, Chengdu University, Chengdu 610106, China; luojie01@cdu.edu.cn
[2] College of Computer Science, Chengdu University, Chengdu 610106, China
* Correspondence: lizhao@cdu.edu.cn; Tel.: +86-183-8207-1390

Abstract: The main purpose of this article is to investigate the dynamic behavior and optical soliton for the M-truncated fractional paraxial wave equation arising in a liquid crystal model, which is usually used to design camera lenses for high-quality photography. The traveling wave transformation is applied to the M-truncated fractional paraxial wave equation. Moreover, a two-dimensional dynamical system and its disturbance system are obtained. The phase portraits of the two-dimensional dynamic system and Poincaré sections and a bifurcation portrait of its perturbation system are drawn. The obtained three-dimensional graphs of soliton solutions, two-dimensional graphs of soliton solutions, and contour graphs of the M-truncated fractional paraxial wave equation arising in a liquid crystal model are drawn.

Keywords: paraxial model; bifurcation; phase portrait; chaos behavior; M-truncated fractional derivative

Citation: Luo, J.; Li, Z. Dynamic Behavior and Optical Soliton for the M-Truncated Fractional Paraxial Wave Equation Arising in a Liquid Crystal Model. *Fractal Fract.* **2024**, *8*, 348. https://doi.org/10.3390/fractalfract8060348

Academic Editor: Carlo Cattani

Received: 22 May 2024
Revised: 3 June 2024
Accepted: 9 June 2024
Published: 12 June 2024

1. Introduction

Fractional partial differential equations (FPDEs) are partial differential equations [1,2] that involve fractional derivatives and are commonly used to describe complex systems with memory effects. FPDEs have wide applications in fluid mechanics, biology, signal processing, and financial mathematics [3]. In general, due to the widespread application of fractional derivatives in multiple fields [4–8], many researchers have proposed many different fractional derivatives from different perspectives. For example, the Riemann–Liouville fractional derivative, the conformable fractional derivative, the Caputo fractional derivative, and the Grünwald–Letnikov fractional derivative. Therefore, with the continuous development of fractional derivative theory, researchers have also delved deeper into the theory of fractional derivatives. Additionally, many different types of FPDEs have been proposed. Due to the complexity and diversity of fractional derivatives, on the one hand, many experts use the finite element method, the spectral method, and the finite difference method to solve the numerical solutions of these equations. On the other hand, many researchers use mathematical analysis methods to construct exact solutions [9,10] to these equations. The main purpose of this article is to study the dynamic behavior and soliton solutions of a very important class of FPDEs.

In this study, the M-truncated fractional paraxial wave equation arising in a liquid crystal model is presented as follows [11]:

$$i\frac{\partial \psi}{\partial y} + \frac{a_1}{2}\,{}_{\kappa}\mathbb{D}_{M,t}^{2\alpha,d}\psi + \frac{a_2}{2}\frac{\partial^2 \psi}{\partial x^2} + a_3|\psi|^2\psi = 0, \tag{1}$$

where a_1, a_2, a_3 are real constants, which represent the coefficients of the dispersal effect, the Kerr nonlinearity effect, and the diffraction effect, respectively. ${}_{\kappa}\mathbb{D}_{M,t}^{2\alpha,d}$ stands for the

M-fractional derivative, which was proposed by Oliveira and Sousa [12]. $\psi = \psi(x, y, t)$, where the variables x, y, t represent the transverse, longitudinal, and temporal propagation, respectively. In [13,14], Hamood, et al. used the ϕ^6 model expansion technique and the Sardar subequation method to study the optical solitons of the paraxial wave model, respectively. In [11], Mannaf et al. studied the optical soliton solutions of Equation (1) by using the extended tanh method and the modified extended tanh method, respectively. However, despite our best efforts, there is still an insufficient body of literature on the dynamic behavior and soliton solutions of Equation (1). Solitons are a special wave phenomenon that occurs in nonlinear physics. Solitons were first proposed in the study of shallow water waves, but were later widely applied in fields such as optics, acoustics, and quantum physics. The optical soliton solution is usually used to describe the mathematical solution of the propagation of optical solitons under specific conditions, for example, the solution to the Schrödinger equation. This article will conduct research from two aspects. On the one hand, by using the method of planar dynamical systems, the dynamic behavior of two-dimensional dynamical systems and their disturbance systems are studied. On the other hand, the optical soliton solution of Equation (1) is constructed using the planar dynamical system method.

The remaining part of this article is arranged as follows: In Section 2, the phase portrait of the two-dimensional dynamical system and its perturbed system are discussed. In Section 3, the optical soliton solutions of Equation (1) are constructed. Finally, a brief conclusion is given.

2. Bifurcation and Chaotic Behaviors

2.1. Preliminary

Definition 1 (M-truncated fractional derivative [15]). *For $\alpha \in (0, 1]$, the M-truncated fractional derivative of $f : [0, +\infty) \to (-\infty, +\infty)$ is defined as*

$$ {}_{\kappa}\mathbb{D}_{M,t}^{2\alpha,d}(f) = \lim_{h \to 0} \frac{f(t_{\kappa}E_d(ht^{\alpha})) - f(t)}{h}, \quad 0 < \alpha < 1, d > 0. $$

In Definition 1, $E_d(z)$ represents the truncated Mittag-Leffler function of one parameter, which is defined as

$$ {}_{\kappa}E_d(z) = \sum_{j=0}^{\kappa} \frac{z^j}{\Gamma(dj+1)}, \; z \in [0, +\infty). $$

M-truncated fractional derivative has very important properties, and relevant conclusions can be referenced in reference [15].

2.2. Mathematical Derivation

Firstly, let us introduce the the wave transformation

$$ \psi(x, y, t) = \Psi(\xi)e^{i\eta}, \xi = m_1 x + m_2 y + \frac{\Gamma(d+1)}{\alpha}\omega t^{\alpha}, \eta = r_1 x + r_2 y + \frac{\Gamma(d+1)}{\alpha}\tau t^{\alpha} + \delta. \tag{2} $$

Inserting Equation (2) into Equation (1), we obtain the real and imaginary components of the resultant expression

$$ \begin{cases} (a_1\omega^2 + a_2 m_1^2)\Psi''(\xi) - 2a_3\Psi^3(\xi) - (a_1\tau^2 + a_2 r_1^2 + 2r_2)\Psi(\xi) = 0, \\ (2a_1\tau\omega + 2a_2 m_1 r_1 + 2m_2)\Psi'(\xi) = 0, \end{cases} \tag{3} $$

where $\Psi'(\xi) \neq 0$.

From the second equation of Equation (3), we have

$$ m_2 = -(a_1\tau\omega + a_2 m_1 r_1). \tag{4} $$

In order to further analyze the dynamic behavior and soliton solutions of Equation (1), under the conditions satisfied by Equation (3), we can transform the first equation of Equation (3) into the following ordinary differential equation:

$$\Psi'' - \Im_1 \Psi^3 - \Im_2 \Psi = 0, \tag{5}$$

Here, $\Im_1 = \frac{2a_3}{a_1\omega^2 + a_2 m_1^2}$ and $\Im_2 = \frac{a_1\tau^2 + a_2 r_1^2 + 2r_2}{a_1\omega^2 + a_2 m_1^2}$, where $a_1\omega^2 + a_2 m_1^2 \neq 0$.

2.3. Qualitative Analysis

The two-dimensional dynamic system of Equation (5) can be described as follows:

$$\begin{cases} \frac{d\Psi}{d\xi} = u, \\ \frac{du}{d\xi} = \Im_1 \Psi^3 + \Im_2 \Psi, \end{cases} \tag{6}$$

with its first integral

$$H(\Psi, u) = \frac{1}{2}u^2 - \frac{\Im_1}{4}\Psi^4 - \frac{\Im_2}{2}\Psi^2 = h. \tag{7}$$

Let $F(\Psi_j) = 0$ ($j = 0, 1, 2$) be the abscissa of the equilibrium point, where $F(\Psi_j) = \Im_1 \Psi_j^3 + \Im_2 \Psi_j$. Assume that $\mathbf{M}(\Psi_j, 0) = \begin{pmatrix} 0 & 1 \\ 3\Im_1 \Psi_j^2 + \Im_2 & 0 \end{pmatrix}$ is the coefficient matrix of (6) at the equilibrium point. Then, we obtain

$$\mathbf{det}(\mathbf{M}(\Psi_j, 0)) = -F'(\Psi_j), j = 0, 1, 2. \tag{8}$$

If $\Im_1 \Im_2 > 0$, system (6) has one equilibrium point $(0, 0)$ (see Figure 1a,b). If $\Im_1 \Im_2 < 0$, the system (6) has three equilibrium points: $(0, 0)$, $(\sqrt{-\frac{\Im_2}{\Im_1}}, 0)$, and $(-\sqrt{-\frac{\Im_2}{\Im_1}}, 0)$ (see Figure 1c,d).

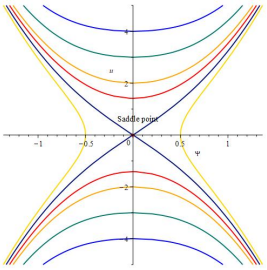

(a) $\Im_1 > 0, \Im_2 > 0$

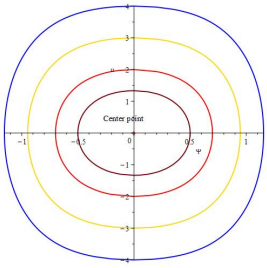

(b) $\Im_1 < 0, \Im_2 < 0$

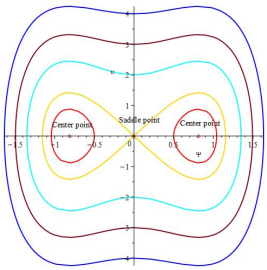

(c) $\Im_1 < 0, \Im_2 > 0$

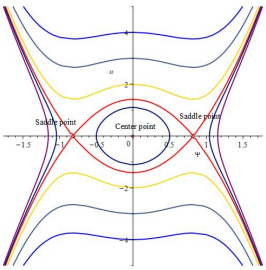

(d) $\Im_1 > 0, \Im_2 < 0$

Figure 1. Two-dimensional phase portrait of system (7).

2.4. Qualitative Analysis with Perturbation Term

In this section, we add the following small perturbation term to system (6):

$$\begin{cases} \frac{d\Psi}{d\xi} = u, \\ \frac{du}{d\xi} = \Im_1\Psi^3 + \Im_2\Psi + f(\xi), \end{cases} \tag{9}$$

where $f(\xi) = A\sin(\varpi\xi)$ and $f(\xi) = Ae^{-0.05\xi}$ are the perturbed terms. A stands for the amplitude of system (9). ϖ is the frequency of system (9).

By fixing the parameters $\Im_1, \Im_2, A, \varpi$, we have drawn the two-dimensional, three-dimensional, and Paincaré section diagrams of system (9), as shown in Figures 2–5. Specifically, when drawing two-dimensional and three-dimensional phase diagrams, we consider the graphs under different initial values. In Figure 6, we plotted the branch phase diagram of system (9) when ϖ takes different values. Obviously, it can be seen from Figure 6 that when A reaches a critical point, the phase diagram of system (9) exhibits chaotic behavior.

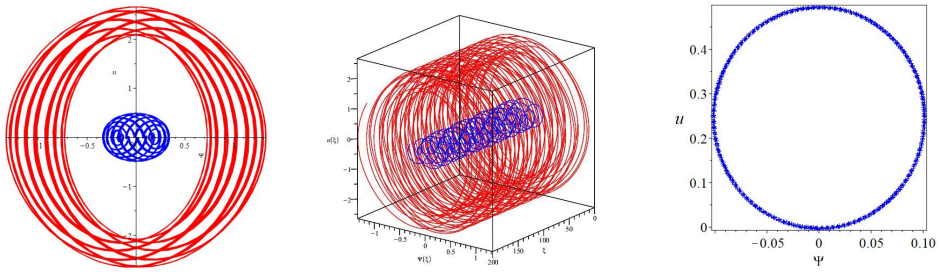

(**a**) 2D phase portrait (**b**) 3D phase portrait (**c**) Paincaré section

Figure 2. The chaotic behaviors of system (9) with $\Im_1 = 1, \Im_2 = -6, A = 1.2, \varpi = 1$.

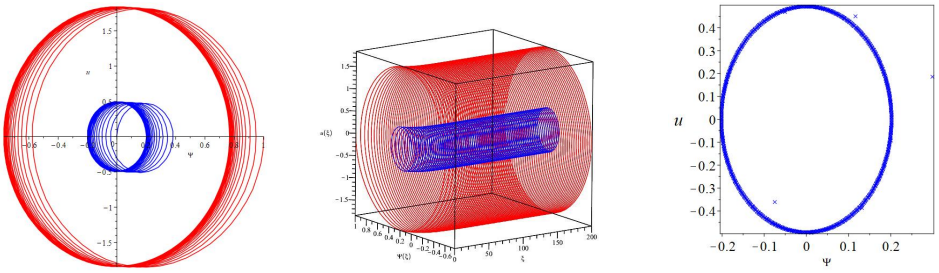

(**a**) 2D phase portrait (**b**) 3D phase portrait (**c**) Paincaré section

Figure 3. The chaotic behaviors of system (9) with $\Im_1 = 1, \Im_2 = -6, A = 1.2$.

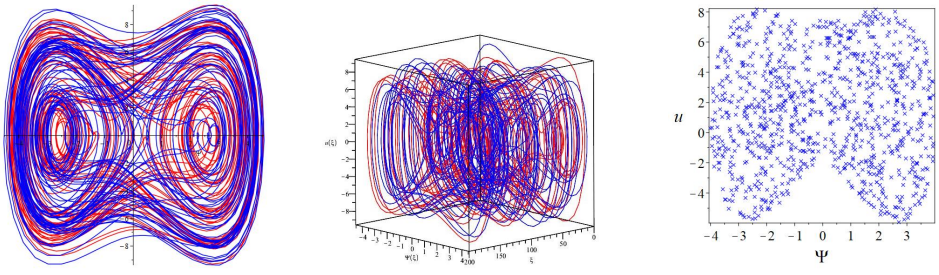

(**a**) 2D phase portrait (**b**) 3D phase portrait (**c**) Paincaré section

Figure 4. The chaotic behaviors of system (9) with $\Im_1 = -1, \Im_2 = 6, A = 6, \varpi = 1$.

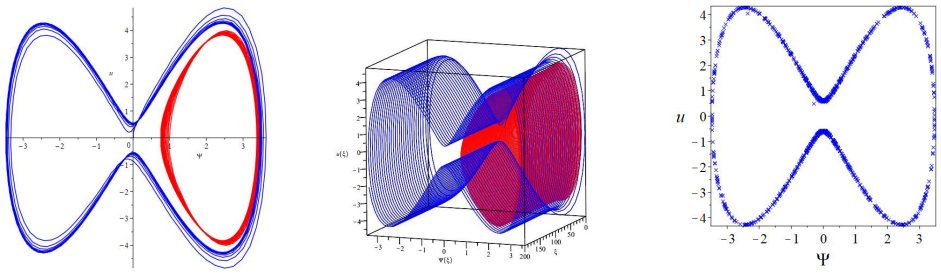

(**a**) 2D phase portrait (**b**) 3D phase portrait (**c**) Paincaré section

Figure 5. The chaotic behaviors of system (9) with $\Im_1 = -1, \Im_2 = 6, A = 1.2$.

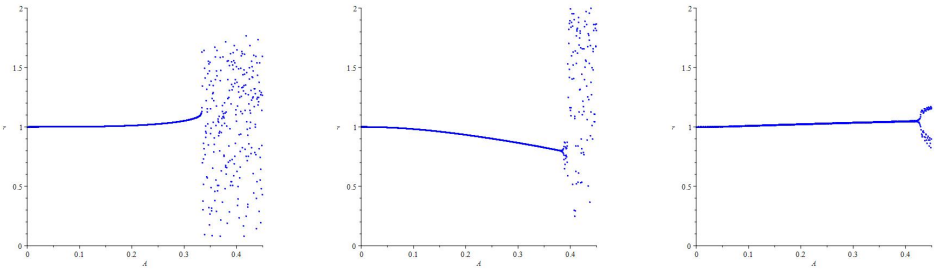

(**a**) $\varpi = \frac{\pi}{8}$ (**b**) $\varpi = \frac{\pi}{4}$ (**c**) $\varpi = \frac{\pi}{2}$

Figure 6. The bifurcation portraits of system (9) with $\Im_1 = -1, \Im_2 = 1, r = \sqrt{u^2 + \Psi^2}$.

3. Optical Soliton Solution of Equation (1)

Let be $h_0 = H(0,0) = 0, h_1 = H(\pm\sqrt{-\frac{\Im_2}{\Im_1}}, 0) = \frac{\Im_2^2}{4\Im_1}$.

3.1. $\Im_1 > 0, \Im_2 < 0, 0 < h < \frac{\Im_2^2}{4\Im_1}$

Then, system (7) becomes

$$u^2 = \frac{\Im_1}{2}(\Psi^4 + \frac{2\Im_2}{\Im_1}\Psi^2 + \frac{4h}{\Im_1}) = \frac{\Im_1}{2}(\varrho_{1h}^2 - \Psi^2)(\varrho_{2h}^2 - \Psi^2), \tag{10}$$

where $\varrho_{1h}^2 = \frac{-\Im_2 + \sqrt{\Im_2^2 - 4\Im_1 h}}{\Im_1}$ and $\varrho_{2h}^2 = \frac{-\Im_2 - \sqrt{\Im_2^2 - 4\Im_1 h}}{\Im_1}$.

Substituting (10) into $\frac{d\Phi}{d\xi} = u$ and integrating it, we can present the Jacobian function solutions

$$\psi_1(x,y,t) = \pm\varrho_{1h}\mathbf{sn}(\varrho_{2h}\sqrt{\frac{\Im_1}{2}}(m_1x + m_2y + \frac{\Gamma(d+1)}{\alpha}\omega t^\alpha), \frac{\varrho_{1h}}{\varrho_{2h}})\mathbf{e}^{i(r_1x + r_2y + \frac{\Gamma(d+1)}{\alpha}\tau t^\alpha + \delta)}. \tag{11}$$

3.2. $\Im_1 > 0, \Im_2 < 0, h = \frac{\Im_2^2}{4\Im_1}$

When $\varrho_{1h}^2 = \varrho_{2h}^2 = -\frac{\Im_2}{\Im_1}$, we can obtain the soliton solution of (1)

$$\psi_2(x,y,t) = \pm\sqrt{-\frac{\Im_2}{\Im_1}}\mathbf{tanh}(\sqrt{-\frac{\Im_2}{2}}(m_1x + m_2y + \frac{\Gamma(d+1)}{\alpha}\omega t^\alpha))\mathbf{e}^{i(r_1x + r_2y + \frac{\Gamma(d+1)}{\alpha}\tau t^\alpha + \delta)}. \tag{12}$$

3.3. $\Im_1 < 0, \Im_2 > 0, -\frac{\Im_2^2}{4\Im_1} < h < 0$

Then, system (7) becomes

$$u^2 = -\frac{\Im_1}{2}(-\Psi^4 - \frac{2\Im_2}{\Im_1}\Psi^2 - \frac{4h}{\Im_1}) = -\frac{\Im_1}{2}(\Psi^2 - \varrho_{3h}^2)(\varrho_{4h}^2 - \Psi^2), \tag{13}$$

where $\varrho_{3h}^2 = \frac{-\Im_2 + \sqrt{\Im_2^2 - 4\Im_1 h}}{\Im_1}$ and $\varrho_{4h}^2 = \frac{-\Im_2 - \sqrt{\Im_2^2 - 4\Im_1 h}}{\Im_1}$.

Substituting (13) into $\frac{d\Phi}{d\xi} = u$ and integrating it, we can present the Jacobian function solutions

$$\psi_3(x,y,t) = \pm\varrho_{4h}\mathbf{dn}(\varrho_{4h}\sqrt{-\frac{\Im_1}{2}}(m_1x + m_2y + \frac{\Gamma(d+1)}{\alpha}\omega t^\alpha), \frac{\sqrt{\varrho_{4h}^2-\varrho_{3h}^2}}{\varrho_{4h}}) \mathbf{e}^{i(r_1x+r_2y+\frac{\Gamma(d+1)}{\alpha}\tau t^\alpha+\delta)}. \tag{14}$$

3.4. $\Im_1 < 0, \Im_2 > 0, h = 0$

When $\varrho_{3h}^2 = 0, \varrho_{4h}^2 == -\frac{2\Im_2}{\Im_1}$, we can obtain the soliton solution of (1)

$$\psi_4(x,y,t) = \pm\sqrt{-\frac{2\Im_2}{\Im_1}}\mathbf{sech}(\sqrt{\Im_2}(m_1x + m_2y + \frac{\Gamma(d+1)}{\alpha}\omega t^\alpha))\mathbf{e}^{i(r_1x+r_2y+\frac{\Gamma(d+1)}{\alpha}\tau t^\alpha+\delta)}. \tag{15}$$

3.5. $\Im_1 < 0, \Im_2 > 0, h > 0$

Then, system (7) becomes

$$u^2 = -\frac{\Im_1}{2}(-\Psi^4 - \frac{2\Im_2}{\Im_1}\Psi^2 - \frac{4h}{\Im_1}) = -\frac{\Im_1}{2}(\varrho_{5h}^2 + \Psi^2)(\varrho_{6h}^2 - \Psi^2), \tag{16}$$

where $\varrho_{5h}^2 = \frac{\Im_2-\sqrt{\Im_2^2-4\Im_1h}}{\Im_1}$ and $\varrho_{6h}^2 = \frac{-\Im_2-\sqrt{\Im_2^2-4\Im_1h}}{\Im_1}$.

Substituting (16) into $\frac{d\Phi}{d\xi} = u$ and integrating it, we can present the Jacobian function solutions

$$\psi_5(x,y,t) = \pm\varrho_{6h}\mathbf{cn}(\sqrt{-\frac{\Im_1(\varrho_{5h}^2+\varrho_{6h}^2)}{2}}(m_1x + m_2y + \frac{\Gamma(d+1)}{\alpha}\omega t^\alpha), \frac{\varrho_{6h}}{\sqrt{\varrho_{5h}^2+\varrho_{6h}^2}}) \mathbf{e}^{i(r_1x+r_2y+\frac{\Gamma(d+1)}{\alpha}\tau t^\alpha+\delta)}. \tag{17}$$

3.6. Numerical Simulations

In this section, we plotted the solutions $\psi_1(x,y,t)$, including the three-dimensional graph, two-dimensional graph, and counter graph, when $a_1 = 1, a_2 = 1, \omega = 1, m_1 = 1, m_2 = 6, \tau = -7, r_1 = 1, r_2 = -\frac{3}{2}, \alpha = \frac{1}{2}, d = 1, h = \frac{3}{16}$ as shown in Figure 7. Obviously, the solution $\psi_1(x,y,t)$ of Equation (1) is a periodic function solution. We plotted the solutions $\psi_2(x,y,t)$, including the three-dimensional graph, two-dimensional graph, and counter graph, when $a_1 = 1, a_2 = 1, \omega = 1, m_1 = 1, m_2 = 6, \tau = -7, r_1 = 1, r_2 = 1, \alpha = \frac{1}{2}$, as shown in Figure 8. Obviously, the solution $\psi_2(x,y,t)$ of Equation (1) is a kink-like soliton. Moreover, we also plot solutions $\psi_3(x,y,t)$, $\psi_4(x,y,t)$, and $\psi_5(x,y,t)$ of Equation (1), as shown in Figures 9–11.

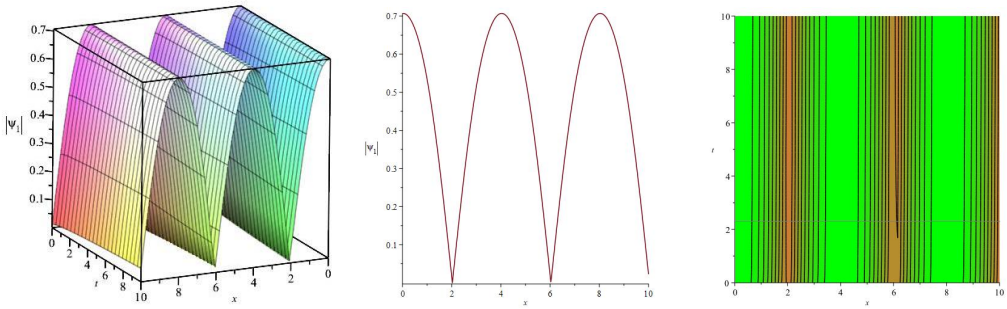

(**a**) 3D graph (**b**) 2D graph (**c**) Contour graph

Figure 7. The solution $\psi_1(x,y,t)$ with $a_1 = 1, a_2 = 1, a_3 = 1, \omega = 1, m_1 = 1, m_2 = 6, \tau = -7, r_1 = 1, r_2 = -25, \alpha = \frac{1}{2}, d = 1, h = \frac{3}{16}$.

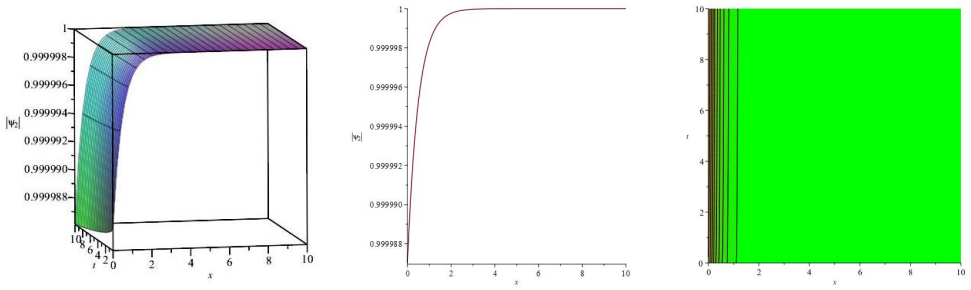

(**a**) 3D graph (**b**) 2D graph (**c**) Contour graph

Figure 8. The solution $\psi_2(x,y,t)$ with $a_1 = 1, a_2 = 1, a_3 = 1, \omega = 1, m_1 = 1, m_2 = 6, \tau = -7, r_1 = 1, r_2 = 1, d = 1, \alpha = \frac{1}{2}, h = \frac{1}{4}$.

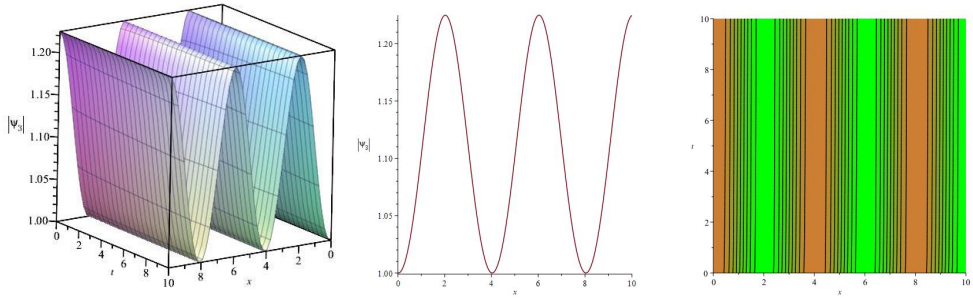

(**a**) 3D graph (**b**) 2D graph (**c**) Contour graph

Figure 9. The solution $\psi_3(x,y,t)$ with $a_1 = 1, a_2 = 1, a_3 = -1, \omega = 1, m_1 = 1, m_2 = 6, \tau = -7, r_1 = 1, r_2 = -24, d = 1, \alpha = \frac{1}{2}, h = -\frac{3}{16}$.

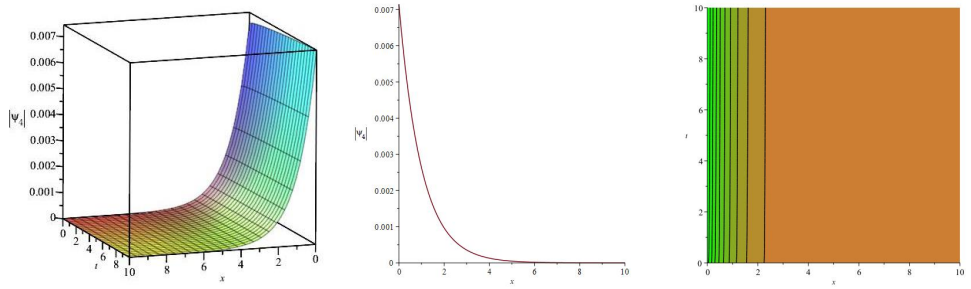

(**a**) 3D graph (**b**) 2D graph (**c**) Contour graph

Figure 10. The solution $\psi_4(x,y,t)$ with $a_1 = 1, a_2 = 1, a_3 = -1, \omega = 1, m_1 = 1, m_2 = 6, \tau = -7, r_1 = 1, r_2 = -24, d = 1, \alpha = \frac{1}{2}, h = 0$.

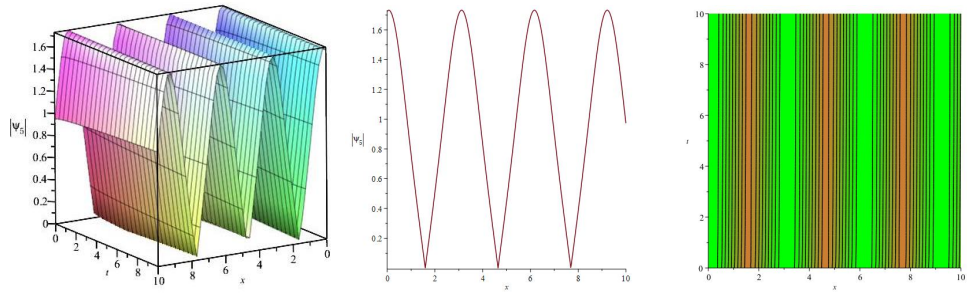

(**a**) 3D graph (**b**) 2D graph (**c**) Contour graph

Figure 11. The solution $\psi_5(x,y,t)$ with $a_1 = 1, a_2 = 1, a_3 = -1, \omega = 1, m_1 = 1, m_2 = 6, \tau = -7, r_1 = 1, r_2 = -\frac{49}{2}, d = 1, \alpha = \frac{1}{2}, h = \frac{3}{4}$.

4. Conclusions

In this article, we use the theory of dynamical systems to study the dynamic behavior and optical soliton for Equation (1) in a liquid crystal model. Furthermore, we used

mathematical software to draw a planar phase diagram of a two-dimensional dynamical system, and we can easily obtain the characteristics of some equilibrium points of the planar dynamical system from the planar phase diagram. And by adding small perturbations, the dynamic behavior of the two-dimensional system is analyzed. Based on different initial values, we have drawn planar phase diagrams using red and blue colors in the same coordinate system. From the perspective of plane dynamics theory, we have drawn a bifurcation phase diagram and Poincaré sections of a disturbance system. And we separately considered the dynamic behavior under periodic and small disturbances. In future research, we will consider the dynamic behavior and optical soliton solutions of more complex FPDEs.

Author Contributions: Software, Z.L.; writing—original draft preparation, J.L.; writing—review and editing, Z.L. All authors have read and agreed to the published version of the manuscript.

Funding: This research received no external funding.

Data Availability Statement: Data are contained within the article.

Conflicts of Interest: The authors declare no conflicts of interest.

References

1. Wu, J.; Yang, Z. Global existence and boundedness of chemotaxis-fluid equations to the coupled Solow-Swan model. *AIMS Math.* **2023**, *8*, 17914–17942. [CrossRef]
2. Wu, J.; Huang, Y.J. Boundedness of solutions for an attraction-repulsion model with indirect signal production. *Mathematics* **2024**, *12*, 1143. [CrossRef]
3. Tang, L. Dynamical behavior and multiple optical solitons for the fractional Ginzburg-Landau equation with β-derivative in optical fibers. *Opt. Quant. Electron.* **2024**, *56*, 175. [CrossRef]
4. Wang, Y.; Qian, Z. Regularizing a two-dimensional time-fractional inverse heat conduction problem by a fractional Landweber iteration method. *Comput. Math. Appl.* **2024**, *164*, 104–115. [CrossRef]
5. Jornet, M. On the Cauchy-Kovalevskaya theorem for Caputo fractional differential equations. *Physica D* **2024**, *462*, 134139. [CrossRef]
6. Yu, J.C.; Feng, Y.Q. On the generalized time fractional reaction-diffusion equation: Lie symmetries, exact solutions and conservation laws. *Chaos Solitons Fractals* **2024**, *182*, 114855. [CrossRef]
7. Espinosa-Paredes, G.; Cruz-López, G.A. A new compartmental fractional neutron point kinetic equations with different fractional orders. *Nucl. Eng. Des.* **2024**, *423*, 113184. [CrossRef]
8. Lu, Y.S.; Hu, Y.Z.; Qiao, Y.; Yuan, M.J.; Xu, W. Sparse least squares via fractional function group fractional function penalty for the identification of nonlinear dynamical systems. *Chaos. Soliton. Fract.* **2024**, *182*, 114733. [CrossRef]
9. Liu, C.Y.; Li, Z. The dynamical behavior analysis and the traveling wave solutions of the stochastic Sasa-Satsuma Equation. *Qual. Theor. Dyn. Syst.* **2024**, *23*, 157. [CrossRef]
10. Gu, M.S.; Chen Peng, C.; Li, Z. Traveling wave solution of (3+1)-dimensional negative-order KdV-Calogero-Bogoyavlenskii-Schiff equation. *AIMS Math.* **2023**, *9*, 6699–6708. [CrossRef]
11. Mannaf, M.A.; Islam, M.E.; Bashar, H.; Basak, U.S.; Akbar, M.A. Dynamical behavior of optical self-control solion in a liquid crystal model. *Results Phys.* **2024**, *57*, 107324. [CrossRef]
12. Usman, Y.; Abdulkadir, S.T.; Ren, J.L. Propagation of M-truncated optical pulses in nonlinear optics. *Opt. Quant. Electron.* **2023**, *55*, 102.
13. Rehman, H.U.; Awan, A.U.; Allahyani, S.A.; Tag-ElDin, E.M.; Binyamin, M.A.; Yasin, S. Exact solution of paraxial wave dynamical model with kerr media by using ϕ^6 model expansion technique. *Results Phys.* **2022**, *42*, 105975. [CrossRef]
14. Rehman, H.U.; Seadawy, A.R.; Younis, M.; Yasi, S.; Raza, S.T.R.; Althobaiti, S. Monochromatic optical beam propagation of paraxial dynamical model in kerr media. *Results Phys.* **2021**, *31*, 105015. [CrossRef]
15. Roshid, M.M.; Uddin, M.; Mostafa, G. Dynamical structure of optical solution for M-fractional paraxial wave equation by using unified technique. *Results Phys.* **2023**, *51*, 106632. [CrossRef]